Title

Electrocautery effects on fluorescence lifetime measurements: An in vivo study in the oral cavity

Authors

Lagarto, João L

Phipps, Jennifer E

Faller, Leta

et al.

Publication Date

2018-08-01

DOI

10.1016/j.jphotobiol.2018.05.025

Peer reviewed

HHS Public Access

Author manuscript

J Photochem Photobiol B. Author manuscript; available in PMC 2019 August 01.

Published in final edited form as:

J Photochem Photobiol B. 2018 August ; 185: 90–99. doi:10.1016/j.jphotobiol.2018.05.025.

Electrocautery effects on fluorescence lifetime measurements: An in vivo study in the oral cavity

João L. Lagarto[a,§], **Jennifer E. Phipps**[a,§], **Leta Faller**[b], **Dinglong Ma**[a], **Jakob Unger**[a], **Julien Bec**[a], **Stephen Griffey**[c], **Jonathan Sorger**[d], **D. Gregory Farwell**[b], and **Laura Marcu**[a,*]

[a]University of California, Davis, Department of Biomedical Engineering, 1 Shields Avenue, Davis, California 95616, United States

[b]University of California, Davis, Department of Otolaryngology-Head and Neck Surgery, 2521 Stockton Boulevard, Suite 7200, Sacramento, California 95817, United States

[c]University of California, Davis, Comparative Pathology Laboratory, 1 Shields Avenue, Davis, California 95616, United States

[d]Intuitive Surgical, 1020 Kifer Road, Sunnyvale, California 94086-5304, United States

Abstract

Tumor removal typically involves electrocautery, but no studies to date have quantified the effect of electrocautery on fluorescence emission. Electrocautery was applied to N=4 locations of the oral cavity and striated leg muscle of a live Yorkshire pig. Autofluorescence of cauterized tissues and surrounding regions was measured at distinct time points up to 120 minutes following cauterization. The fluorescence lifetime was spectrally resolved in four spectral detection channels that maximized the signal emanating from endogenous fluorophores of interest. The autofluorescence emission (355 nm excitation) was temporally resolved using a high-speed digitizer; resulting fluorescence decay characteristics were retrieved using the Laguerre deconvolution technique. Histology was performed and co-registered with the autofluorescence data. Results show that cauterized tissue presents a distinct autofluorescence signature from surrounding regions immediately after cauterization. Differences become less evident with time. The autofluorescence-derived parameters suggest altered metabolism in peripheral regions compared to the region of maximal damage. Within the time-frame of this study, tissues investigated show variable degrees of recovery from the effects of electrocautery that can be monitored by changes in fluorescence lifetime characteristics. Our findings suggest delineation of pathologic conditions could be affected by tissue cauterization and that future studies in this area will be necessary.

*Laura Marcu, lmarcu@ucdavis.edu.
§Indicates joint authorship, authors contributed equally to this work

Supporting Information

Additional supporting information may be found in the online version of this article at the publisher's website.

Disclosures

Jonathan Sorger is an employee and stockholder of Intuitive Surgical, Inc.

Keywords

fluorescence lifetime spectroscopy and imaging; robotic surgery; cauterization; autofluorescence; wound healing

1 Introduction

Electrocautery is a process that applies high-frequency alternating current to generate heat in living tissues to make surgical cuts or provide hemostasis.[1] While electrical cauterization of tissues can provide enhanced hemostasis compared to alternate approaches, thermal energy generated during cauterization may dissipate to adjacent tissues and promote extensive inflammation and injury.[2,3] Electrocautery is used widely for surgical procedures across various clinical specialties. With the advent of fluorescence techniques also being applied in intraoperative tissue diagnosis e.g.,[4–7] it is important to determine the effect cautery has on the fluorescence properties of tissue.

A key challenge in cancer resection surgeries is often associated with the inability of the surgeon to visibly see the tumor and thus to accurately define resection margins. The ability to distinguish cancer from normal surrounding tissues is of paramount importance to improve patient outcomes and thus many techniques are currently being investigated towards that end, including fluorescence lifetime. Multispectral autofluorescence lifetime spectroscopy is a promising label-free tool that can report on structural and biochemical alterations in tissue owing to pathological transformations by resolving the fluorescence decay dynamics of endogenous molecules of interest such as collagens, elastin, NAD(P)H and FAD. Since it is inherently ratiometric, autofluorescence lifetime is relatively insensitive to intensity artifacts that affect other techniques, such as fluorophore concentration or excitation/collection geometry.[8] The potential and feasibility of this technique for in vivo clinical diagnosis have been demonstrated in a number of studies, e.g.[5–7,9] Hence, when combined with fiber-based instruments, autofluorescence lifetime measurements could enhance intraoperative diagnosis and provide guidance in surgical procedures.

Despite the numerous studies showing the potential of autofluorescence lifetime measurements to report contrast between cancer and normal tissues, there are still challenges that need to be addressed before this technique can be routinely used in surgical settings. One question that remains unanswered refers to whether autofluorescence lifetime can detect tumor margins in cauterized tissue following resection. Resection of a tumor implicates excision beyond the obvious tumor margins. In superficial cancers, the trained eye and experience of the surgeon serves as the only guide to identify the resection margins. In cases where cancer extends deep into the tissue, it is challenging to predict the depth of the cancerous region and therefore the safe margins for resection, which could lead to incomplete resection of the tumor. Therefore, a technique that could guide surgeons and help identify cancer margins in cauterized tissues would have obvious benefits that could impact patient outcomes.

Here we study the effect of cautery on autofluorescence lifetime measurements from normal tissue as a first step towards understanding whether autofluorescence lifetime spectroscopy

can resolve pathological conditions in cauterized tissue resected margins. The number of studies reporting the use of autofluorescence in cauterized or burnt tissues is still limited[10–12] and therefore our goal is to characterize the autofluorescence signature of different tissues following cauterization, within the time frame of a typical cancer resection surgery. In particular, we aim to establish a baseline readout for multispectral autofluorescence measurements of cauterized normal tissues that could serve as a reference for non-cancerous resection margins during in vivo studies. Given our interest in the real-time detection of oral cancer in surgical settings, we report the application of a multispectral fiber-optic based time-resolved fluorescence spectroscopy instrument that was incorporated with the da Vinci Surgical System (Intuitive Surgical, California, USA) to investigate the autofluorescence characteristics of different tissues of the oral tract of swine in vivo. Although our investigation is confined to a case study from a healthy animal, it provides new and important insights into the autofluorescence signature of cauterized tissues.

2 Methods

2.1 Animal model

Based on prior robotic research studies, a female 65 kg Yorkshire pig was used for this study due to the morphological similarities in the oral mucosa between human and pig. Additionally, the animal is large enough to allow for the da Vinci Surgical System to be used for the electrocautery and autofluorescence measurements, closely mimicking our intended clinical use. The procedure was performed with the appropriate Institutional Animal Care and Use Committee approval.

2.2 Experimental setup

To study the effects of cauterization on the autofluorescence signature of tissue, the surface of four different locations in the oral tract of a pig were cauterized: base of tongue, tonsil, an intersection between tonsil and soft palate (tonsil + soft palate), and tongue. To mimic the deeper muscular tissues found in the mouth following resection of tumors, the surface of the left adductor muscle was also cauterized. Cauterization of tissues was performed using the Intuitive Surgical EndoWrist® monopolar flat blade cautery instrument via the da Vinci system. In vivo autofluorescence lifetime measurements were carried out for each location before and at different time points following cauterization, as indicated in Fig, 1. The pig was anesthetized during the entire duration of the procedure.

2.3 Optical Instrumentation

Experiments described in this study were carried out using a custom-built fiber-based multispectral fluorescence lifetime imaging (FLIm) system depicted in Fig. 2 and previously described in detail elsewhere.[13,14] Excitation light at 355 nm was provided by a frequency-tripled micro Q-switched Nd:Yag laser (Teem Photonics, France, 600 ps pulse width, 2 kHz repetition rate) and delivered to the sample via a single 400 μm core diameter silica fiber (Polymicro TechnologiesTM, USA) that was also used to collect the fluorescence emanating from the sample. At the collection end, the fiber was coupled to a wavelength selection module consisting of a set of dichroic mirrors and band-pass filters that provided spectrally resolved detection of the autofluorescence signal. The spectral bands were selected to

maximize the autofluorescence signal from endogenous fluorophores of interest, namely collagen (390 ± 20 nm, channel 1), NAD(P)H (470 ± 14 nm, channel 2), FAD (542 ± 25 nm, channel 3) and porphyrins (629 ± 26.5 nm, channel 4). The four detection channels were connected to optical fibers of different lengths that provided a time delay of approximately 60 ns between consecutive channels. At the distal end, the fibers were directed into a single microchannel plate photomultiplier tube (MCP-PMT, R3809U-50, Hamamatsu, 45 ps FWHM). The output of the MCP-PMT was connected to a 3 GHz bandwidth amplifier (AM-1607–3000, Miteq, USA) to amplify the autofluorescence signal before reaching the high-speed digitizer (PXIe-5185, National Instruments, 12.5 GS/s sampling rate), where the signal was temporally resolved at 80 ps intervals.

To create autofluorescence images from this single-point instrument, a CW 450 nm laser diode (PL 450B, Osram, Germany) is used to produce a blue aiming beam that is visible with the white light camera incorporated in the robot, as shown in Fig. 3B. A complete description of this method was recently published elsewhere.[17] Briefly, since the projected aiming beam can provide an approximate position of the origin of the autofluorescence signal, segmentation of the aiming beam from the white light image allows determination of the (x, y) coordinates for each autofluorescence measurement. By performing segmentation of the aiming beam in real-time in parallel with deconvolution of the autofluorescence decay, FLIm maps can be created and super-impose with the white light image from the robot. In this manner, augmented images are generated as the data as acquired and visible in the da Vinci surgeon console. Figure 3C shows an example of a white light image of the soft palate captured with the da Vinci camera and augmented with channel 1 autofluorescence lifetime data.

2.4 Data analysis

The autofluorescence decay characteristics for each set of pixels within the segmented aiming beam region were retrieved by deconvolving the instrument response function (IRF) with the Laguerre basis functions, as previously described.[15] Given the sensitivity of intensity measurements to excitation/collection geometry and probe-to-target distance, the autofluorescence intensity in each spectral channel was calculated as a fraction of the total autofluorescence signal, i.e. the sum of all detection channels. When two measurements produced overlapping aiming beam regions, the autofluorescence intensity ratios and lifetimes within these regions were averaged.

In order to quantify the metabolic activity of the tissue, we calculated the optical redox ratio *RR*.[17] In our instrument, NADH and FAD autofluorescence can be detected in channels 2 and 3, respectively, although NADH is also expected to contribute significantly to channel 3 autofluorescence, given the excitation wavelength used in our measurements (λ_{exc} = 355 nm) and the broad emission spectrum of NADH.[18] Collagen also yields a broad emission spectrum that could contribute to the autofluorescence signal in channels 2 and 3 [19]. However, at 355 nm excitation, collagen emission peaks at 400–415 nm [20,21] and has low autofluorescence intensity at the wavelength range of channels 2 and 3 compared to NADH and FAD autofluorescence. Therefore, the redox ratio from the normalized ratio of

autofluorescence intensities measured in channels 2 and 3 is calculated as shown in Eq. 1 below.

$$RR = \frac{I_{CH2}}{I_{CH2} + I_{CH3}} \sim \frac{[NADH]}{[NADH] + [FAD]} \quad (1)$$

To quantify the autofluorescence lifetime variations throughout the time, three regions of interest (ROIs) of approximately 20 × 20 px were selected from each white light image, following Jackson's burn wound model[16] (see Fig. 3). Regions were selected from the cauterized tissue (charred), the edge of cauterization (border) and a distant region (remote), approximately 1 cm away from the cauterized region. Before cauterization, a single and wider region of interest (approximately 20 × 60 px) was selected, to account for the intrinsic variability of tissue. The autofluorescence lifetime in each region was determined by averaging all pixels within the region.

2.5 Histology

Imaged tissues were harvested post-mortem for histology sectioning and analysis approximately 8 hours after the measurements due to experimental constraints and in accordance with the reduction principle of animal research. Upon harvesting, tissues were fixed in 10% neutral-buffered formalin and routinely processed for paraffin embedding. 4 μm thick sections were cut from the paraffin blocks and stained for hematoxylin and eosin. Representative histology images of base of tongue, muscle and tonsil are presented in Fig. 3D and in the supplement for all locations investigated.

3 Results

Following cauterization, a distinct charred region was clearly visible where tissue was cauterized, presenting a similar pattern to that previously described by Jackson[16] (Fig. 3A). Below we present results for base of tongue, tonsil and muscle. For base of tongue, we present a more comprehensive description of the data, including white light images at the time of measurements. Given that we observed similar results in all anatomical locations investigated, data for tonsil and muscle are presented as a summary. Maps of all autofluorescence lifetime and intensity parameters are provided in the supplement for all time points and regions studied, along with representative histology images.

3.1 Base of tongue.

Figures 4 and 5 in the cauterized region and remote regions. In particular, the region of cauterization can be well demarcated from remote regions for up to 33 minutes. In this timeframe, the cauterized region demonstrates a shorter autofluorescence lifetime in channels 1, 2 and 3 (Fig. 4), decreased relative autofluorescence intensity in channels 1 and 3 (Fig. 5). It is relevant to point out that the autofluorescence signal detected in channel 4 was typically very low (see supplement) giving rise to artifacts in the deconvolution process and noisy autofluorescence lifetime images. Notably, the differences observed in the autofluorescence signal directly after cauterization tend to normalize with time, resulting in

the region of cauterization no longer being distinct from remote regions at later time points. The fluorescence intensity at later time points is different from baseline, which suggests metabolic activity in the sampled area that potentially relates to the process of tissue recovery following cautery (also evident in Fig. 5). In general, we observe an increase in the measured autofluorescence lifetime in all spectral channels and time points relative to baseline, although this is more evident in remote regions. At 87 minutes, the autofluorescence lifetimes are similar to baseline values, although we also observe a relative increase in the measured lifetime at 118 minutes. These trends can be observed in Fig. 6. This fluctuation is also present in the intensity parameters associated with NADH and FAD autofluorescence (see redox ratio below) and therefore suggests modulation of the metabolic activity, potentially related to the inflammatory response of the tissue [22,23]. With respect to the autofluorescence intensity data, our results indicate a red-shift in the fluorescence emission in the cauterized region, which contrasts with remote regions, where we see an increase in relative autofluorescence in channel 1.

3.2 Tonsil

Similar autofluorescence patterns to those of BOT were found in tonsil measurements (see Fig. 7), where we observe a clear differentiation between cauterized and remote regions up to 16 minutes after cauterization, which is followed by slow dissipation of these differences. In the baseline measurement, our data show significant variations in the autofluorescence signature, in particular in the intensity parameters, which can be explained by variations in tissue composition. Histologic examination of this sample revealed the presence of connective tissue (see blue arrow, in Fig. 7) adjacent to tonsillar lymphatic tissue. The most abundant sources of autofluorescence in connective tissue are collagens and to a lesser extent elastin fibers,[24] which explains the autofluorescence signature in this region, given the long autofluorescence lifetime of collagen and its strong autofluorescence intensity in the emission band of our detection channel 1. [19,20,25,26] With respect to the variation of the autofluorescence lifetime with time, we observed similar trends to BOT in detection channels 2 and 3, i.e. an increase in autofluorescence lifetime in all regions investigated relative to baseline values. In contrast, channel 1 autofluorescence lifetime decreases in the charred area upon cauterization and in regions in the immediate vicinity, while in remote regions we observe an increase in the lifetime up to 16 minutes, followed by a decrease. At 16 minutes, the lifetime difference in channel 1 between remote and charred regions was found to be 1.150 ± 0.108 ns (mean ± SD), which decreased to 0.001 ± 0.195 ns at t = 30 min. This rapid shift in the autofluorescence lifetime in remote regions along with the increasingly homogeneous autofluorescence signature may be associated to metabolic accommodation of the viable tissue potentially as an inflammatory response to the cautery damage and to maintain viability of the most affected regions. As with BOT, the autofluorescence signature of tonsil appears to become more homogeneous with time, following an initial period of evident differentiation between the charred area and its surroundings.

3.3 Muscle

Of all tissues investigated, muscle was the only tissue type presenting clear differentiation of the charred region throughout the entire duration of the study (i.e. 45 minutes), as our results

demonstrate in Fig. 8. In general, the results show a decrease in autofluorescence lifetime in channel 1 in the charred area, which contrasts with the increase observed in border and remote regions. In detection channels 2 and 3, the lifetime in remote and charred regions shows opposite trends: in the cauterized region, the lifetime increases with time following cauterization; in remote regions, the lifetime increases immediately after the cauterization reaching a relative maximum at 4 minutes and decreases after this time point. This variation in the autofluorescence signature may be associated to the presence of fat in tissue (pointed out by the blue arrow in Fig. 8) that has distinct autofluorescence properties compared to muscle.

3.4 Redox ratio.

The redox ratio quantifies the level of oxidative phosphorylation over glycolysis in tissue by comparing the autofluorescence of NADH and FAD, which are well-known fluorophores intimately involved in these metabolic pathways. Upregulation of glycolysis leads to production of NADH at a faster rate than FAD is produced during oxidative phosphorylation, which leads to impairment of the cellular levels of these metabolites.[27] The results presented in Fig. 9 show a consistent increase in redox ratio in remote regions relative to baseline values in all anatomical locations investigated. Furthermore, results also show a consistently higher redox ratio in remote regions compared to charred tissue, suggesting higher metabolic activity in remote regions due to the greater accumulation of NADH and thus upregulation of the glycolytic pathway. In BOT (see Fig. 9, left plot), our data suggests similar metabolic activity throughout the tissue at 118 minutes, which further suggests recovery of the tissue following cauterization. Although data for tonsil and muscle data also suggest balanced metabolic activity throughout the tissue over time, this is not as evident, which is potentially related to the shorter duration of the studies.

4 Discussion

Autofluorescence lifetime spectroscopy and imaging provides a label-free and non-destructive means to report structural and biochemical alterations in tissue owing to pathological transformations. Accordingly, its potential for intraoperative tissue diagnosis has been explored and demonstrated in a number of studies, with emphasis on cancer identification and resection margins delineation.[5–7,28,29] While autofluorescence lifetime measurements have been shown to provide means of distinguishing between normal and cancer tissue, it remains unclear whether they can provide similar contrast when tissues are altered by surgical procedures such as electrocautery. As a first approach to address this question, we characterized the autofluorescence properties of cauterized non-cancerous tissue with the aim of establishing a baseline for in vivo studies. This baseline can serve as reference for comparison with cauterized tissues during resection surgery, which could potentially improve the identification of cancerous tissue in cauterized regions following resection. Our results point to a number of interesting findings, in particular: 1) cauterized regions present a distinct autofluorescence signature from remote non-cauterized tissues immediately after cauterization; 2) changes in redox ratio, NAD(P)H and FAD autofluorescence parameters in remote regions suggest altered metabolism; 3) differences in

autofluorescence parameters tend to fade away with time, suggesting accommodation of the tissue to cauterization.

General anesthesia can promote a series of physiological events such as altered blood pressure and respiratory rate, which may have an impact on tissue metabolism [30,31] and, likewise, on tissue autofluorescence characteristics. While the impact of anesthesia in the fluorescence properties of tissues has not been investigated in depth, we believe it does not have a significant influence in our observations. Our baseline measurements (i.e. pre-cautery) were realized under anesthesia and thus can serve as control, permitting a direct comparison of the tissue autofluorescence properties before and after cauterization, given the time scale of our studies. Furthermore, autofluorescence measurements would follow a similar protocol in the context of a cancer resection surgery since those measurements would occur under anesthesia before and after cancer resection.

According to Jackson's burn wound model,[16] burn injuries are characterized by three concentric regions, as depicted in Fig. 3A: the region of maximum damage (i.e. directly affected by the burn trauma) is called zone of coagulation and is characterized by vascular occlusion and consequent necrosis and irreversible tissue lost; surrounding this region is a transition zone called the zone of stasis, which is characterized by decreased blood perfusion that could lead to necrosis; the periphery of the burn is called the zone of hyperemia and it is characterized by vasodilation with consequent increase in blood perfusion due to the production of inflammatory mediators. Similar regions to those identified by Jackson can be observed from our autofluorescence data, which demonstrate clear separation of the regions immediately after cauterization of all tissues investigated. Our histology data (see supplemental data) reveals the presence of necrotic tissue in cauterized regions, which is consistent with previous literature.[16,32] However, it is relevant to point out that tissue for histology was harvested several hours after imaging of the sample due to experimental constraints and therefore it may not be representative of the state of the tissue at time of measurements, particularly with respect to the distribution of inflammatory cells.

One factor that is important to take into account is the temperature of the tissue. It is known that the autofluorescence lifetime of NAD(P)H and FAD decreases linearly with temperature.[33,34] We are inducing thermal damage and thus it is possible that our results are, to some extent, affected by a slight increase in tissue temperature, particularly at earlier time points. However, we note that increase in temperature applied during cautery is expected to dissipate rapidly (< 1 minute), thus before the earliest measurement (3 minutes). Furthermore, vasodilation resulting from damage will increase microcirculatory blood flow, thus dissipating heat more effectively. Clearly, differentiation between charred and remote tissues can still be observed up to 45 minutes after cauterization as in the case of muscle (Fig. 8). At this time point, the heat generated during cauterization is completely dissipated, which suggests that changes in tissue autofluorescence are mostly reflecting biochemical and structural alterations as result of the inflammatory response rather than thermal changes.

Consistently we observe a decrease in channel 1 absolute autofluorescence intensity in the area of maximal damage (data not shown). At 355 nm excitation, the autofluorescence signal emanating from oral tissues is dominated by NAD(P)H and FAD fluorescence in non-

keratinized epithelium and collagen fluorescence in stroma.[35] Similar autofluorescence signature is expected from skeletal muscle.[36] In some locations of the oral mucosa where keratinized stratified squamous epithelium is found, such as tongue (see supplemental data), keratin can also have a relevant contribution to the autofluorescence signal. At 355 nm excitation, keratin has a similar spectral profile to that of collagen and therefore can make the interpretation of the autofluorescence signal more challenging.[35] Given the penetration depth of light at 355 nm (~200 μm) and through co-registration with histology, we observe that our autofluorescence signal emanates predominantly from the most superficial layer of the oral cavity, with varying contribution from the stroma underneath depending upon the thickness of the oral mucosa. The mucosa is very cellular whereas the stroma has high collagen content. Therefore changes observed in channel 1 are likely to be generated by both alterations in metabolism (from NAD(P)H and FAD autofluorescence) and structural proteins (keratin in keratinized epithelium and collagen in non-keratinized epithelium) caused by cautery. Overall, our results demonstrate that changes in the autofluorescence properties of tissue follow similar trends, irrespective of the tissue structure and biochemical composition. In contrast, the magnitude and times at which these changes occur may be influenced by tissue composition. The inflammatory response of the tissue to thermal trauma promotes immediate changes in microcirculation leading to edema, red blood cells and scattered leukocytes in tissue, as observed in our histology data. In particular, vasodilation promotes formation of localized edema in the extracellular space, which leads to sparser distribution of the cellular layers. Given our fiber optic detection scheme, we are unable to report such microscopic changes in tissue morphology in detail. Rather, changes in the autofluorescence signal due to morphological or biochemical alterations are averaged out within the excitation-collection volume. Leukocytes exhibit strong autofluorescence between 450 and 500 nm, which overlaps well with the autofluorescence emission of free and bound NAD(P)H.[37–39] Immediately upon cauterization we observe a shift in the autofluorescence emission towards shorter wavelengths in remote regions, which could be indicative of the accumulation of leukocytes. This result is further supported by redox ratio measurements (Fig. 9) that also demonstrate favoring of glycolysis and a concomitant change in metabolism in remote regions compared to the charred region. An increase in metabolic activity is expected in the zone of hyperemia at the earliest stages of inflammation following thermal injury as an attempt of tissue to maintain viability of the most affected regions.[40] The differences between charred and remote regions tend to fade away with time in all anatomical locations investigated except for muscle, which suggests sparse distribution of leukocytes throughout the tissue and homogeneous metabolic activity at later time points. The observation that the signal did not normalize in muscle was possibly because of the shorter duration of the protocol compared to other tissues. If more measurements were carried out at later time points, the autofluorescence signature of charred and remote regions would likely become increasingly homogenous as for the base of tongue around 33 minutes and tonsil around 16 minutes. We also observed a sparse distribution of leukocytes in our histology images (data not shown), with predominance in the region of cauterization, although at the time that tissue was harvested for histology (approximately 8 hours after starting the measurements) inflammation would have been at a more advanced state than that depicted by our data that was acquired at an earlier time point.

With respect to the autofluorescence lifetime data, we observe a consistently shorter lifetime in the charred region compared to remote regions, although this is most pronounced in channel 1. Cauterization of tissue can lead to denaturation of structural proteins (e.g collagen and its cross-links) as well as proteins that bind to NAD(P)H, which typically exhibit fluorescence emission at shorter wavelengths and longer lifetimes compared to free-NAD(P)H.[18,41] Hence, it is possible that the autofluorescence lifetime shift that we observe in channel 1 is to some extent reflecting an alteration of collagen and crosslinks and an increase in free-NAD(P)H content relative to protein bound NAD(P)H. In the base of tongue, we observed a general increase in the autofluorescence lifetime of all detection channels relative to baseline values and in all regions of interest (see Fig. 4 and 6). The latest time points in the study are similar to baseline values, and this is also observed in tonsil for detection channels 2 and 3 (Fig. 7). The similarity observed in the autofluorescence lifetime signature of these two regions may be associated to their prominent lymphatic composition covered by stratified squamous epithelium at the surface.[42] Our histologic images of tonsil indicated the presence of connective tissue in superficial layers, which can be well distinguished in the autofluorescence images, denoting a longer fluorescence lifetime and stronger emission in channel 1 (see Fig. 7, blue arrow). The distinct autofluorescence properties of connective tissue compared to those of tonsil may have dominated the autofluorescence lifetime readout of channel 1, which could explain the differences observed in tonsil and base of tongue in this channel that are not observed in channels 2 and 3. In general, we observed similar lifetime trends across the different spectral channels of our instrument. While the information provided by each channel does not seem to be complimentary in the context of the current experiment, we note that this is typically not the case in a cancer measurement, where the autofluorescence information is relevant and distinct across the entire visible spectrum. Therefore, we consider as being relevant to present the multispectral autofluorescence signature of cauterized tissue in the context of a cancer measurement.

Similarly, histologic images of muscle revealed the presence of fat at the surface of the tissue. Autofluorescence emanating from fat cells is mostly visible in channel 1, as determined via histology co-registration and visualized by a longer lifetime and stronger emission in this band (see Fig. 8). The heterogeneous composition of this tissue is likely to be causing the fluctuations in the lifetime signature of channels 2 and 3, as demonstrated in Fig.8. In general, results demonstrate clear differentiation between charred and remote regions throughout the entire duration of the measurements. This contrasts with results obtained for other tissues where differences between charred and remote regions become less evident. This can potentially be explained by the shorter duration of the measurements in muscle compared to other tissues. However, our data also shows that at 30 minutes after cauterization, charred and remote regions of tonsil cannot be distinguished, while we still observe prominent differences between these regions in muscle at later time points. These differences could be associated with the composition of the tissue that would give rise to different recovery times, potentially associated to the metabolic rate. It could also be associated to the extent of the thermal damage, i.e. cauterization of the muscle could have caused more damage compared to other tissues, which could lead to extended recovery periods. The time and temperature of cauterization were not consistent for each location.

Hence, to understand the homogeneity observed in the autofluorescence signature of different tissues and the rates at which they occur, further studies are necessary, potentially exploring animal models where the severity of the lesion can be more carefully controlled.

The sample size (one swine) is a limitation of this study, which we mitigate by measuring multiple sites and tissues. While these locations are not identical in composition, they all presented similar autofluorescence signatures following cauterization, which is a promising indicator that we could take these into account when imaging cauterized tissues during surgery. In the future, we intend to expand these studies to include animal models of cancer, which would allow us to investigate reproducibility across samples and could potentially offer a more definitive answer regarding the ability of autofluorescence lifetime measurements to distinguish cancer within resection margins.

5 Conclusion

This study reports on the characterization of the autofluorescence intensity and lifetime signatures of different tissues following thermal damage. The main goal of this study was to evaluate the variation of the autofluorescence signal following cauterization of different tissues, with a view to understand whether autofluorescence could be used to identify pathological transformations within resection margins of charred tissue. Current results have demonstrated that the fluorescence parameters derived from measurements in vivo following exposure to electrocautery undergo significant changes as a function of time and are tissue type dependent. Based on this case study alone, it is unclear the exact time tissue autofluorescence properties return to the initial conditions (i.e. prior to cautery). Current results indicate that this time varies with tissue type and overall exceeds 30 minutes. Additional studies are needed to reproducibly determine a more precise recovery time for each tissue type and to evaluate whether the time scale of these observations is compatible with the time frame of a surgery. In general, our results suggest that changes in tissue following cauterization could be well characterized using intensity data alone, which would suppress the need for expensive lifetime instrumentation. However, in the context of cancer measurements, the autofluorescence signature is typically more complex given the multitude of fluorophores modulating the signal and underlying competing biological mechanisms. Thus, in such conditions, fluorescence lifetime data can provide an extra dimension to the optical readout and aim to distinguish fluorophores that are otherwise undistinguishable.

While further studies will be necessary to determine whether autofluorescence parameters can be robustly used to distinguish cancer within resection margins in vivo following cautery, our current study identifies potential challenges for the use and interpretation of optical parameters for tissue characterization when cautery is used. In addition, one important question that this study raises refers to the viability of ex vivo optical measurements in tissue following electrosurgical resection. Considering the extended exposure to thermal damage that tissue typically endures in cancer resection surgeries, ex vivo optical measurements should take into account the considerable impact of cauterization in the optical properties of tissue and subsequent use of such properties for the identification of positive margins.

Moreover, the current study provides a framework for future work that will focus on evaluation of fluorescence measurements to associate metabolic related signals with histology data at different time points. In particular, it would be interesting to understand the complex autofluorescence signatures in later time points (i.e. > 2 hours), potentially up to a few weeks after cauterization, to study structural and functional alterations in tissue during burn wound repair. Current methods to track progress of burn wound healing remain largely based on visual inspection by the clinical support team [23] and thus non-invasive imaging parameters such as those provided by fluorescence lifetime measurements could be explored to accurately monitor structural and functional progress of burn wound healing process and potentially help clinicians during treatment. Hence, this work can potentially open new pathways of research, with particular emphasis to wound healing research and tissue regeneration.

In conclusion, tissue fluorescence properties undergo dynamic changes following cauterization. This model suggests that autofluorescence changes induced by cautery stabilize in a finite period of time, but this length of time may vary based on tissue type, cautery parameters and even species. As such, definitive recommendations cannot be made at this point about when autofluorescence measurements begin to indicate tissue composition rather than changes in metabolic activity due to cautery. This will be the focus of future investigations that can benefit from the observations reported in the current study. Furthermore, we compiled a list of questions the current study has raised that merit exploration before fluorescence techniques, or any other optical technique sensitive to transitory changes in tissue optical properties in response to cautery and heat, are further adopted in the clinical setting: 1) to what extent is the surrounding tissue affected by cautery? How deep? How wide? 2) How much time does it take for tissue to biologically and metabolically recover from cautery and will it recover within a clinically relevant time frame to a new normal or to the pre-cautery state? 3) How does the energy applied to the tissue via cautery affect the biological and metabolic properties of tissue and how long will the tissue take to recover in respect to time and intensity of the applied cautery? 4) How are ex vivo resected tissue specimens affected by cautery and are they reliable indicators of their in vivo state (diseased or normal) prior to cautery?

Supplementary Material

Refer to Web version on PubMed Central for supplementary material.

Acknowledgements

We would like to acknowledge assistance from Dale Bergman and Katrina Lau at Intuitive Surgical for assistance during the experiment. We would also like to acknowledge funding from Intuitive Surgical and the NIH R01 CA187427. Authors 1 and 2 contributed equally to this work.

References

1. Hasar ZB, Ozmeric N, Ozdemir B, et al. Comparison of Radiofrequency and Electrocautery With Conventional Scalpel Incisions. J Oral Maxillofac Surg. 2016;74(11):2136–2141. doi:10.1016/j.joms.2016.06.172. [PubMed: 27424067]

2. Liboon J, Funkhouser W, Terris DJ. A comparison of mucosal incisions made by scalpel, CO2 laser, electrocautery, and constant-voltage electrocautery. Otolaryngol - Head Neck Surg. 1997;116(3): 379–385. doi:10.1016/S0194-5998(97)70277-8. [PubMed: 9121794]

3. Yilmaz KB, Dogan L, Nalbant H, et al. Comparing scalpel, electrocautery and ultrasonic dissector effects: The impact on wound complications and pro-inflammatory cytokine levels in wound fluid from mastectomy patients. J Breast Cancer. 2011;14(1):58–63. doi:10.4048/jbc.2011.14.1.58. [PubMed: 21847396]

4. Mayinger B, Jordan M, Horbach T, et al. Evaluation of in vivo endoscopic autofluorescence spectroscopy in gastric cancer. Gastrointest Endosc. 2004;59(2):191–198. doi:10.1016/S0016-5107(03)02687-7. [PubMed: 14745391]

5. Thompson AJ, Coda S, Sørensen MB, et al. In vivo measurements of diffuse reflectance and time-resolved autofluorescence emission spectra of basal cell carcinomas. J Biophotonics. 2012;5(3): 240–54. doi:10.1002/jbio.201100126. [PubMed: 22308093]

6. Coda S, Thompson AJ, Kennedy GT, et al. Fluorescence lifetime spectroscopy of tissue autofluorescence in normal and diseased colon measured ex vivo using a fiber-optic probe. Biomed Opt Express. 2014;5(2):515–38. doi:10.1364/BOE.5.000515. [PubMed: 24575345]

7. Kantelhardt SR, Kalasauskas D, Konig K, et al. In vivo multiphoton tomography and fluorescence lifetime imaging of human brain tumor tissue. J Neurooncol. 2016;127(3):473–482. doi:10.1007/s11060-016-2062-8. [PubMed: 26830089]

8. Marcu L Fluorescence lifetime techniques in medical applications. Ann Biomed Eng. 2012;40(2): 304–31. doi:10.1007/s10439-011-0495-y. [PubMed: 22273730]

9. Fatakdawala H, Poti S, Zhou F, et al. Multimodal in vivo imaging of oral cancer using fluorescence lifetime, photoacoustic and ultrasound techniques. Biomed Opt Express. 2013;4(9):1724. doi: 10.1364/BOE.4.001724. [PubMed: 24049693]

10. Vo LT, Anikijenko P, McLaren WJ, Delaney PM, Barkla DH, King RG. Autofluorescence of skin burns detected by fiber-optic confocal imaging: evidence that cool water treatment limits progressive thermal damage in anesthetized hairless mice. J Trauma. 2001;51(1):98–104. Available at: http://www.ncbi.nlm.nih.gov/pubmed/11468475. [PubMed: 11468475]

11. Lin M-G, Yang T-L, Chiang C-T, et al. Evaluation of dermal thermal damage by multiphoton autofluorescence and second-harmonic-generation microscopy. J Biomed Opt. 2006;11(6):64006. doi:10.1117/1.2405347.

12. Kaiser M, Yafi A, Cinat M, Choi B, Durkin AJ. Noninvasive assessment of burn wound severity using optical technology: A review of current and future modalities. Burns. 2011;37(3):377–386. doi:10.1016/j.burns.2010.11.012. [PubMed: 21185123]

13. Yankelevich DR, Ma D, Liu J, et al. Design and evaluation of a device for fast multispectral time-resolved fluorescence spectroscopy and imaging. Rev Sci Instrum. 2014;85(3):34303. doi: 10.1063/1.4869037.

14. Gorpas D, Ma D, Bec J, Yankelevich D, Marcu L. Real-Time Visualization of Tissue Surface Biochemical Features Derived from Fluorescence Lifetime Measurements. IEEE Trans Med Imaging. 2016;62(c):1–1. doi:10.1109/TMI.2016.2530621.

15. Liu J, Sun Y, Qi J, Marcu L. A novel method for fast and robust estimation of fluorescence decay dynamics using constrained least-squares deconvolution with Laguerre expansion. Phys Med Biol. 2012;57(4):843–65. doi:10.1088/0031-9155/57/4/843. [PubMed: 22290334]

16. Jackson DM. The diagnosis of the depth of burning. Br J Surg. 1953;40(164):588–596. doi: 10.1002/bjs.18004016413. [PubMed: 13059343]

17. Chance B, Cohen P, Jobsis F, Schoener B. Intracellular oxidation-reduction states in vivo. Science (80-). 1962;137(3529):499–508. Available at: http://www.ncbi.nlm.nih.gov/pubmed/4398818.

18. Lakowicz JR, Szmacinski H, Nowaczyk K, Johnson ML. Fluorescence lifetime imaging of free and protein-bound NADH. Proc Natl Acad Sci U S A. 1992;89(4):1271–5. Available at: http://www.pubmedcentral.nih.gov/articlerender.fcgi?artid=48431&tool=pmcentrez&rendertype=abstract. [PubMed: 1741380]

19. Lagarto J, Dyer BT, Talbot C, et al. Application of time-resolved autofluorescence to label-free in vivo optical mapping of changes in tissue matrix and metabolism associated with myocardial

infarction and heart failure. Biomed Opt Express. 2015;6(2):324. doi:10.1364/BOE.6.000324. [PubMed: 25780727]

20. Manning HB, Nickdel MB, Yamamoto K, et al. Detection of cartilage matrix degradation by autofluorescence lifetime. Matrix Biol. 2013;32(1):32–8. doi:10.1016/j.matbio.2012.11.012. [PubMed: 23266527]
21. Lewis W, Padilla-Martinez JP, Ortega-Martinez A, Franco W. Changes in endogenous UV fluorescence and biomechanical stiffness of bovine articular cartilage after collagenase digestion are strongly correlated. J Biophotonics. 2016;8:1–8. doi:10.1002/jbio.201600093.
22. Tiwari V Burn wound: How it differs from other wounds? Indian J Plast Surg. 2012;45(2):364. doi: 10.4103/0970-0358.101319. [PubMed: 23162236]
23. Rowan MP, Cancio LC, Elster E a, et al. Burn wound healing and treatment: review and advancements. Crit Care. 2015;19(1):243. doi:10.1186/s13054-015-0961-2. [PubMed: 26067660]
24. Paulsen F, Thale A. Epithelial-connective tissue boundary in the oral part of the human soft palate. J Anat. 1998;193 (Pt 3:457–67. doi:10.1046/j.1469-7580.1998.19330457.x. [PubMed: 9877301]
25. Moise N, Carp C, Pascu M-L. Laser-induced fluorescence of collagen and cholestrol. In: Vlad VI, ed. Vol 2461; 1995:386. doi:10.1117/12.203579.
26. Wagnieres GA, Star WM, Wilson BC. In Vivo Fluorescence Spectroscopy and Imaging for Oncological Applications. Photochem Photobiol. 1998;68(5):603–632. doi:10.1111/j. 1751-1097.1998.tb02521.x. [PubMed: 9825692]
27. Tzagoloff A. Mitochondria. Plenum Press; 1982 Available at: http://books.google.co.uk/books?id=gl_wAAAAMAAJ.
28. Mycek M-A, Schomacker KT, Nishioka NS. Colonic polyp differentiation using time-resolved autofluorescence spectroscopy. Gastrointest Endosc. 1998;48(4):390–394. [PubMed: 9786112]
29. Sun Y, Phipps JE, Meier J, et al. Endoscopic Fluorescence Lifetime Imaging for In Vivo Intraoperative Diagnosis of Oral Carcinoma. Microsc Microanal. 2013:791–798. [PubMed: 23702007]
30. Sumi C, Okamoto A, Tanaka H, et al. Propofol induces a metabolic switch to glycolysis and cell death in a mitochondrial electron transport chain-dependent manner. PLoS One. 2018;13(2):1–22. doi:10.1371/journal.pone.0192796.
31. Kishikawa J ichi, Inoue Y, Fujikawa M, et al. General anesthetics cause mitochondrial dysfunction and reduction of intracellular ATP levels. PLoS One. 2018;13(1):1–12. doi:10.1371/journal.pone. 0190213.
32. Teot L, Otman S, Brancati A, Mittermayr R. Burn Wound Healing: Pathophysiology. Handb Burn. 2012:47–54.
33. Scott TG, Spencer RD, Leonard NJ, Weber G. Emission Properties of NADH. Studies of Flurorescence Lifetimes and Quantum Efficiencies of NADH, AcPyADH, and Simplified Synthetic Models. J Am Chem Soc. 1970;7302(1968).
34. Whal P, Auchet JC. Time Resolved Fluorescence of Flavin Adenine Dinucleotide. FEBS Lett. 1974;44(1):67–70. [PubMed: 4855213]
35. Wu Y, Qu JY. Autofluorescence spectroscopy of epithelial tissues. J Biomed Opt. 2006;11(5): 54023. doi:10.1117/1.2362741.
36. Schilders SP, Gu M. Three-dimensional autofluorescence spectroscopy of rat skeletal muscle tissue under two-photon excitation. Appl Opt. 1999;38(38):720–723. [PubMed: 18305669]
37. Monici M, Pratesi R, Bernabei P a, et al. Natural fluorescence of white blood cells: spectroscopic and imaging study. J Photochem Photobiol B. 1995;30:29–37. doi:10.1016/1011-1344(95)07149-V. [PubMed: 8558361]
38. Goertz O, Vogelpohl J, Jettkant B, et al. Burn model for in vivo investigations of microcirculatory changes. Eplasty. 2009;9:e13. [PubMed: 19412334]
39. Blacker TS, Mann ZF, Gale JE, et al. Separating NADH and NADPH fluorescence in live cells and tissues using FLIM. Nat Commun. 2014;5(May):3936. doi:10.1038/ncomms4936. [PubMed: 24874098]
40. Hettiaratchy S, Dziewulski P. Pathophysiology and types of burns. Br Med J. 2004;328(June): 1427–1429. doi:10.1136/bmj.328.7453.1427. [PubMed: 15191982]

41. Palero JA, Bader AN, de Bruijn HS, der Ploeg van den Heuvel A Van, Sterenborg HJCM, Gerritsen HC. In vivo monitoring of protein-bound and free NADH during ischemia by nonlinear spectral imaging microscopy. Biomed Opt Express. 2011;2(5):1030–9. doi:10.1364/BOE.2.001030. [PubMed: 21559117]

42. Fang WS, Wiggins RH, Illner a., et al. Primary Lesions of the Root of the Tongue. Radiographics. 2011;31(7):1907–1922. doi:10.1148/rg.317095738. [PubMed: 22084179]

Highlights

- Fluorescence lifetime measurements in a pig demonstrate effects of electrocautery
- Tissue presents distinct autofluorescence immediately after cauterization
- Electrocautery autofluorescence effects on tissue dissipate over time
- Fluorescence studies during surgery must consider electrocautery effects

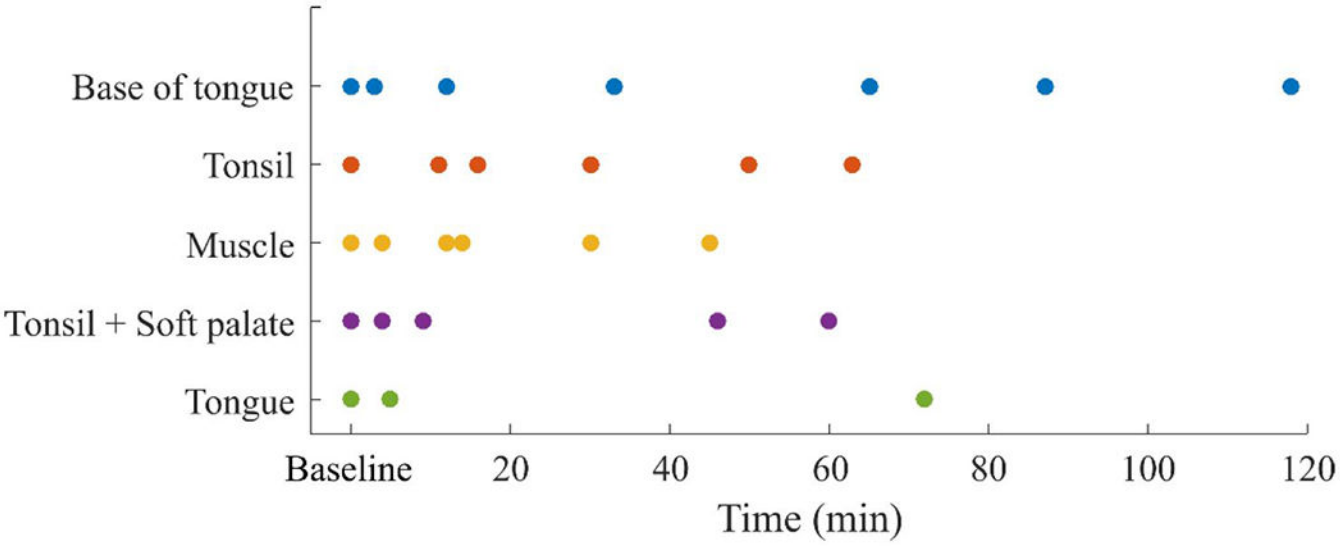

Figure 1.
Diagram depicting time of measurements for each anatomical location investigated. Results for tonsil + soft palate and tongue are presented in the supplement.

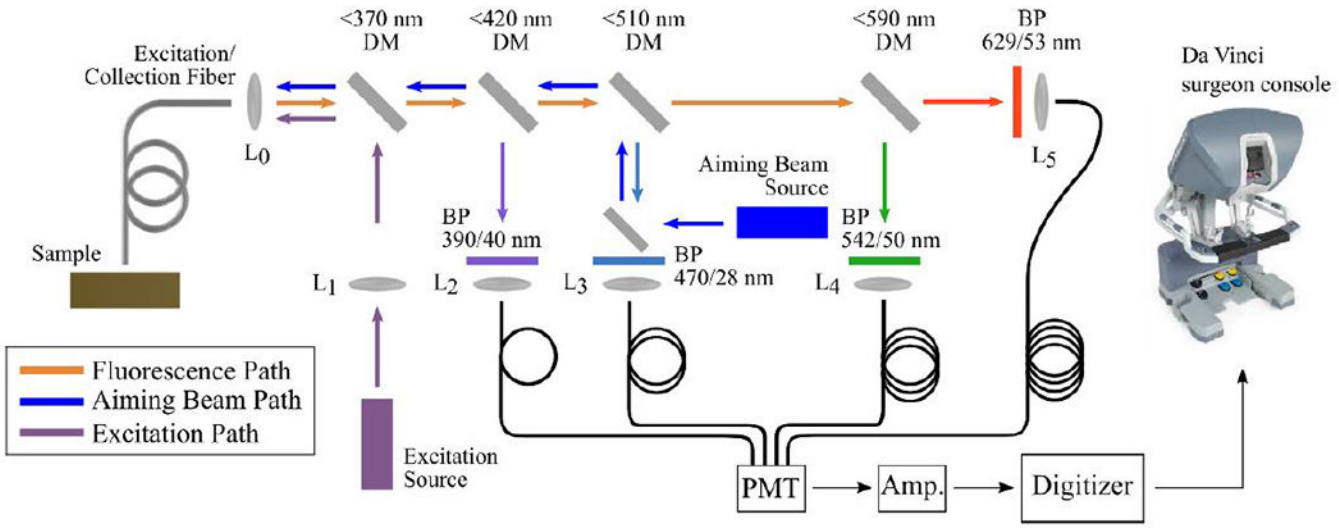

Figure 2.

Experimental layout of the fiber based fluorescence lifetime imaging system. The distal end of the optical fiber was fitted to a 5-French introducer that was mounted in one of the instrument arms of the da Vinci Surgical System.

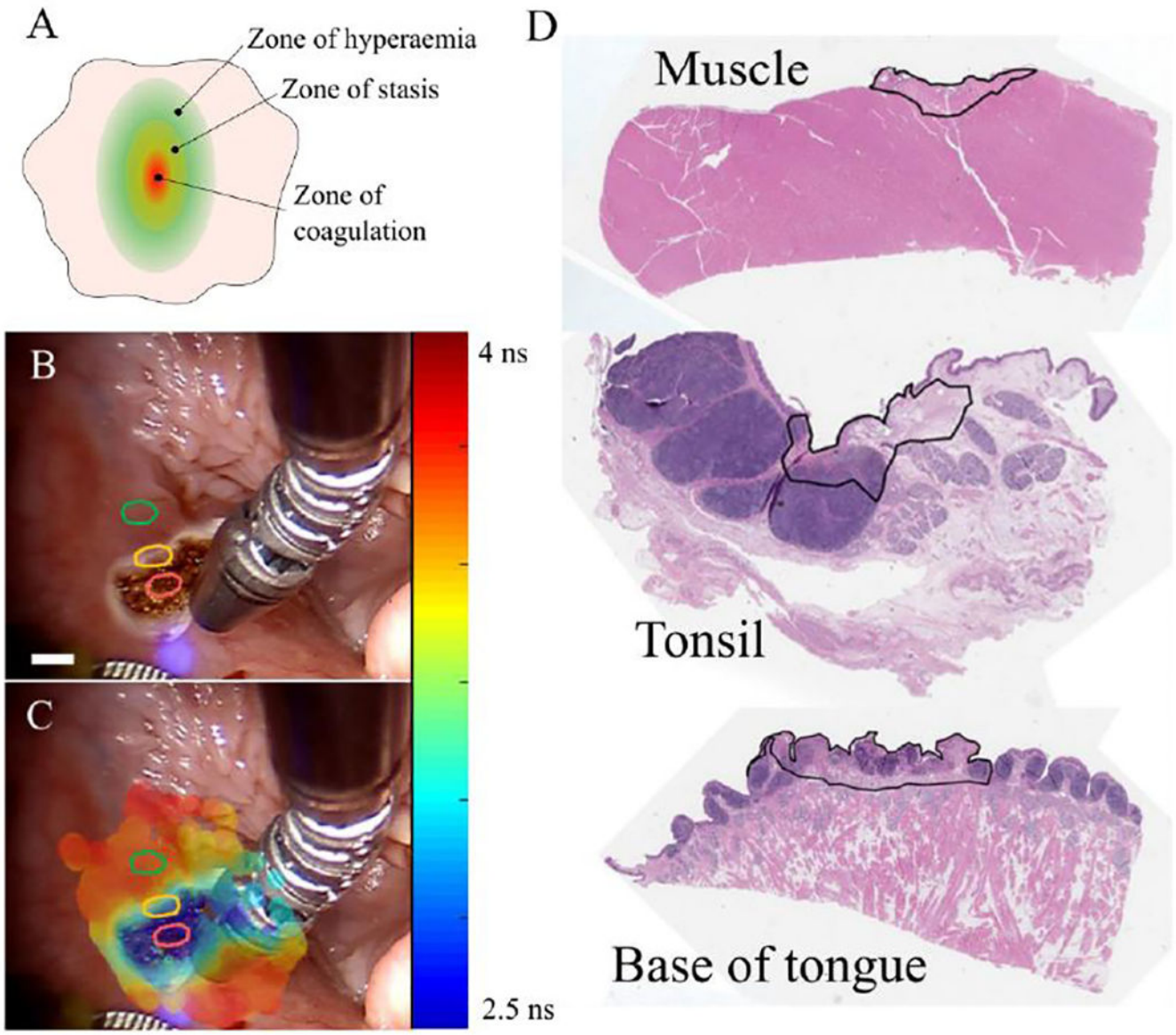

Figure 3.

A) Simplified schematic of the burnt zones according to the Jackson's burn wound model[16]. B) White light image of cauterized tissue (t = 4 min) during a FLIm acquisition and (C) corresponding augmented image with channel 1 fluorescence lifetime data. Red, yellow and green regions identify charred, border and remote areas, respectively. Similar regions of interest were identified in the base of tongue, tongue and tonsil for comparison of the autofluorescence lifetime parameters at different time points. Scale bar ~3 mm at the sample. D) Representative histology images muscle, tonsil and base of tongue. Delineated regions identify areas of cellular necrosis following cauterization.

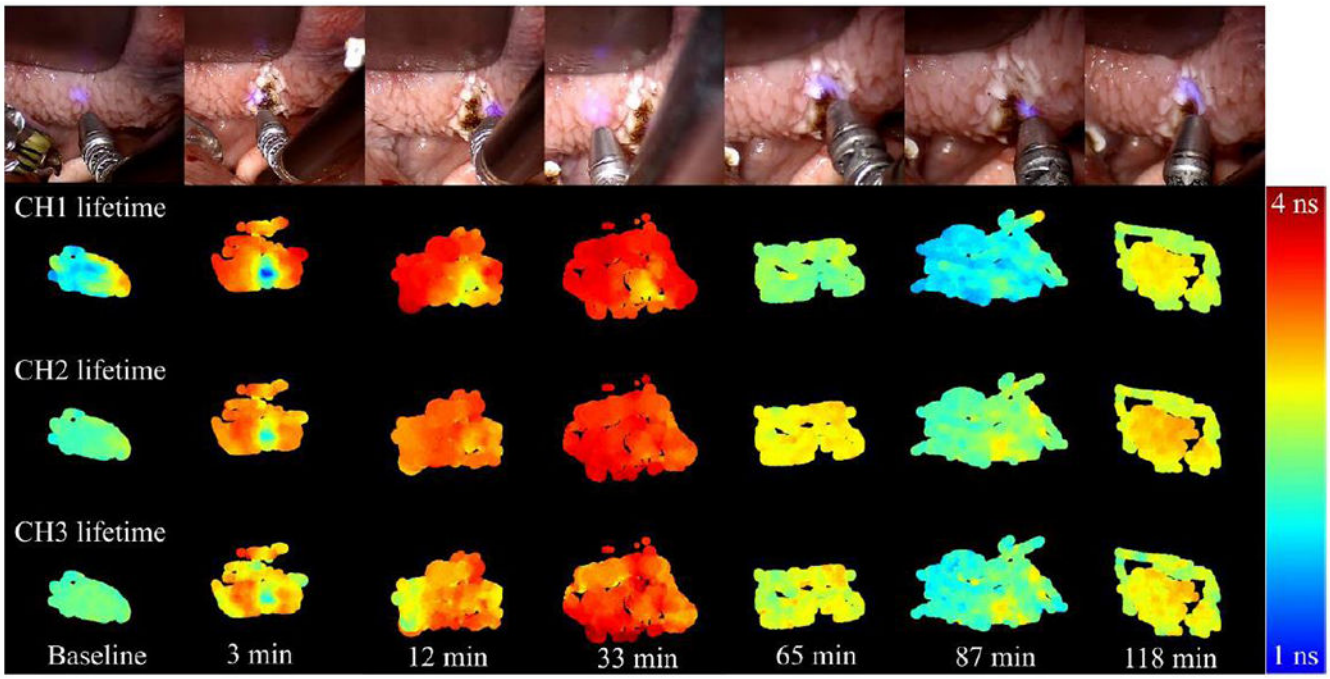

Figure 4.

Base of tongue autofluorescence lifetime maps (channels 1, 2 and 3) for baseline and all time points following cauterization of the tissue. Top row shows white light images captured with the da Vinci Surgical System at the time of measurement.

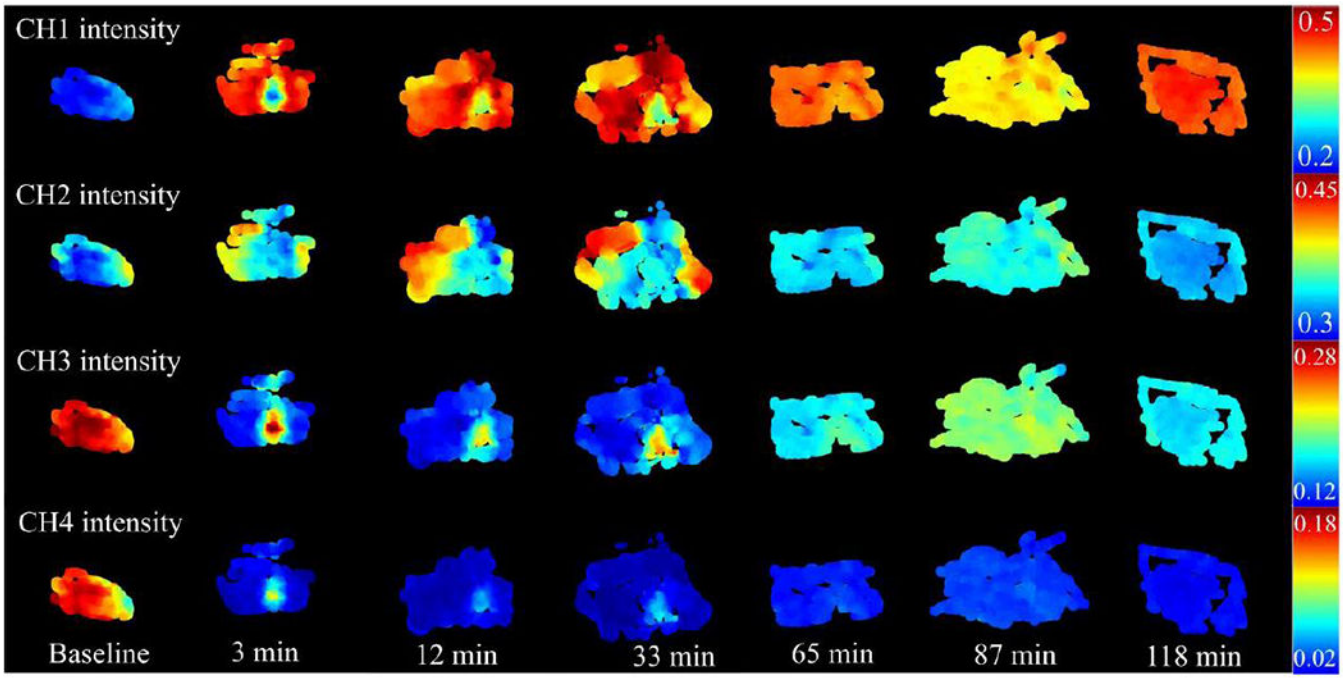

Figure 5.
Normalized autofluorescence intensity maps of all detection channels for base of tongue.

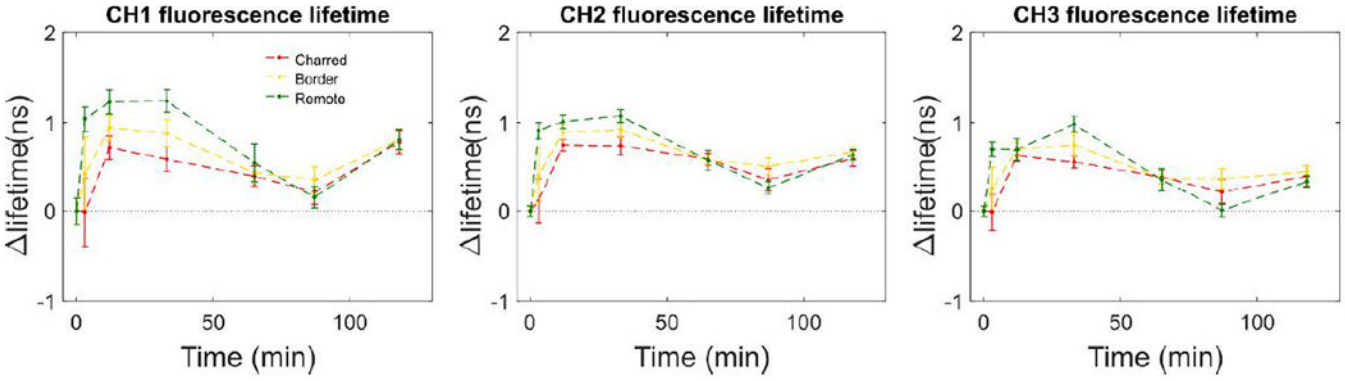

Figure 6.

Variation of autofluorescence lifetime with time after cauterization of base of tongue tissue for each ROI. At each time point, results are presented as the difference in autofluorescence lifetime between that time point and baseline measurements (i.e. t = 0 min).

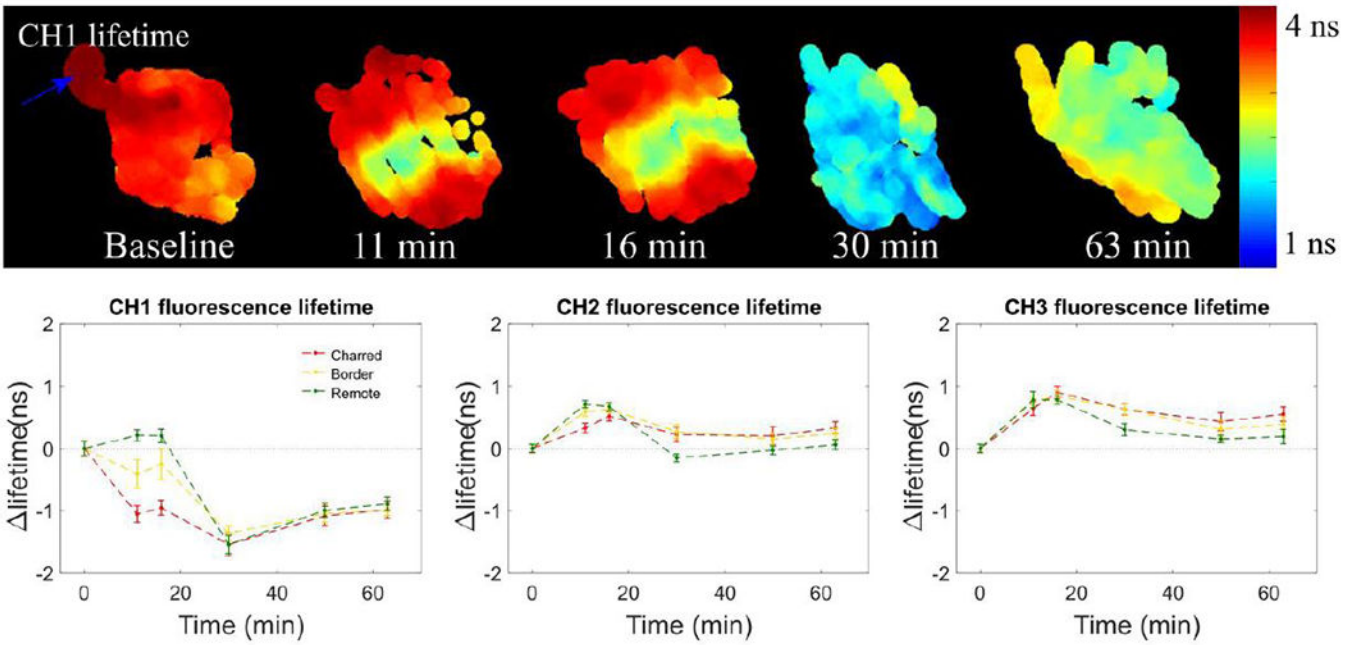

Figure 7.

Summary of tonsil FLIm measurements for baseline and different time points following cauterization of the tissue, showing clear differentiation of the cauterized region. Maps of all autofluorescence lifetime and intensity parameters are provided in the supplement for all time point studied. Plots at the bottom show curves of the variation of autofluorescence lifetime with time after cauterization of the tissue for each ROI. At each time point, results are presented as the difference in autofluorescence lifetime between that time point and baseline measurements (i.e. t = 0 min).

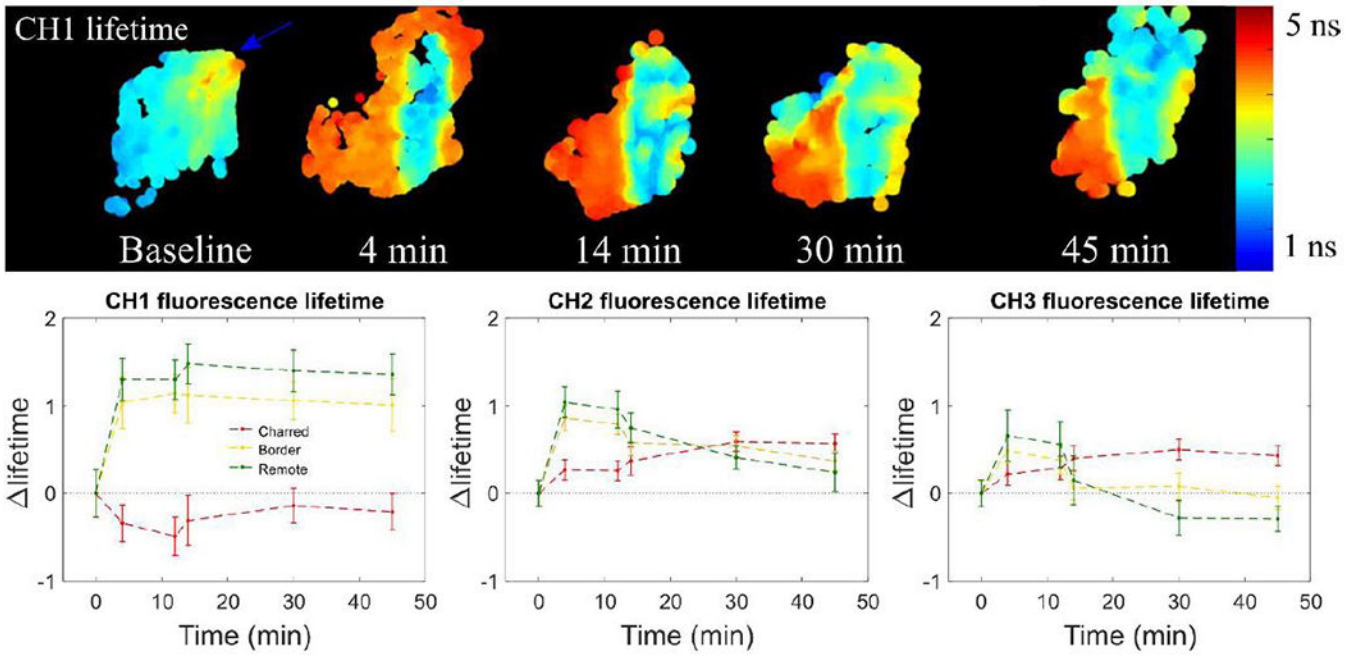

Figure 8.

Summary of muscle measurements for baseline and different time points following cauterization of the tissue depicted through channel 1 autofluorescence lifetime. Maps of all autofluorescence lifetime and intensity parameters are provided in the supplement for all time points studied.

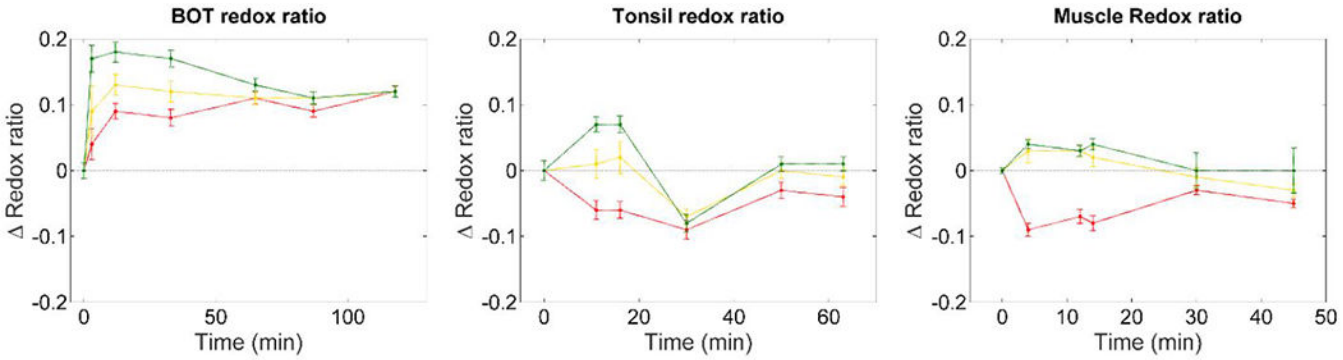

Figure 9.

Variation of redox ratio with time – calculated as $I_{CH2}/(I_{CH2} + I_{CH3})$ – for all anatomical locations of interest. At each time point, results are presented as the difference in redox ratio at that time relative to the baseline value (i.e. t = 0 min). Data show increased redox ratio in remote regions immediately after cauterization of the tissue and up to 80 minutes after cauterization (see BOT, left plot), which suggests altered metabolism in these regions.